International Journal of Basic and Applied Sciences, 14 (5) (2025) 625-638

International Journal of Basic and Applied Sciences

Website: www.sciencepubco.com/index.php/IJBAS
https://doi.org/10.14419/t62an110
Research paper

Content Subtle Style Generative Adversarial Network with Multitask Efficient NetB7 to Predict Embryo Ploidy Status for Effective IVF Outcomes

S. Divya [1] *, S. Geetharani [2]

[1] Department of Computer Science, PSG College of Arts and Science, Coimbatore-641014, Tamil Nadu, India
[2] Department of Computer Technology, PSG College of Arts and Science, Coimbatore-641014, Tamil Nadu, India
**Corresponding author E-mail: divyamyu123phd@gmail.com*

Received: July 15, 2025, Accepted: August 22, 2025, Published: September 17, 2025

Abstract

Usually, the assisted reproductive units prevent multiple pregnancies by transferring a single embryo. Experts should choose an embryo to transplant from a unit created by the intended parents. This selection technique must be precise, non-intrusive, reliable, and accessible to In-Vitro Fertilization (IVF) facilities globally. However, the key challenge is determining embryo ploidy status and choosing the most viable embryos for successful transfer. To address this issue, embryo genetic status is assessed via Preimplantation Genetic Testing for Aneuploidy (PGT-A), which entails embryo biopsy and genetic testing. However, it is invasive and costly. As a result, non-invasive techniques using Machine Learning (ML) and Deep Learning (DL) models are created to estimate embryo ploidy status from time-lapse embryo photos, allowing for decision-making before further treatment. Conversely, these models frequently rely on low-quality and insufficient numbers of embryo images as well as a lack of clinical and demographic information about the patient, such as age, pelvic factor, sperm count, etc., resulting in decreased accuracy. For augmenting embryo images, Generative Adversarial Network (GAN) and its variant called Style-based GAN (StyleGAN) were applied; yet, they were restricted to producing images with low resolutions, leading to poor image quality. Hence, this article develops a novel Content Subtle Style-based GAN (CSSGAN) with a Multi-model EfficientNetB7 (MENB7) model to augment time-lapse embryo images and predict ploidy status for effective IVF outcomes. The CSSGAN adopts content-aware channel pruning and content-sensitive distillation approaches as minimax optimization tasks to generate a massive quantity of high-quality and high-fidelity human embryo images at the blastocyst stage. The generated images are input into the Mask-Residual Convolutional Neural Network (Mask-RCNN) for segmentation. Then, the relevant features from the segmented images are captured by EfficientNetB7, which fuses them with the patient's clinical and demographic data to create a unified feature vector. Moreover, a Fully Connected (FC) layer with softmax is used for predicting euploid and aneuploid embryos. Finally, extensive experiments using distinct datasets illustrate the efficiency of the CSSGAN-MENB7 model in predicting embryo ploidy status with 95.88% accuracy compared to the conventional DL models.

Keywords: *EfficientNetB7, Embryo ploidy prediction, IVF, Mask-RCNN, Non-invasive, PGT, StyleGAN,*

1. Introduction

In earlier decades, embryo morphology was the sole tool for determining the quality and capability of an embryo [1]. Since euploid embryos with an appropriate human chromosomal complement of 46 chromosomes are linked to better medical results, they are usually chosen for transfer over aneuploid embryos with an inappropriate complement. So, finding and choosing a high-quality embryo for transfer is essential to increase the pregnancy probability. For this purpose, embryo selection techniques using morphokinetic embryonic characteristics have emerged based on static and morphological criteria. However, morphology alone cannot guarantee an effective implantation event or a euploid embryo [2]. Based on a combined genetic and morphological analysis of blastocyst and cleavage embryos, genetic irregularities did not significantly impact morphology until day three of growth; many of these embryos still reached the maximum morphological grade [3]. Numerous academics have evaluated the influence of morphologic time points and time to development of aneuploidy rates as time-lapse imaging platforms have grown in popularity [4]. Morphokinetic parameter assessment has not increased the probability of choosing euploid embryos [5]. As well, variability in embryo morphologic assessment remains a key issue in learning and standardizing decisions made by experts based on morphology.

The PGT-A and Next-Generation Sequencing (NGS) have sparked a genetic advancement that will continue to expand and influence embryo selection. Randomized controlled trials have revealed that shifting PGT-A-tested euploid embryos increases the pregnancy

possibility of women aged 35 to 40 compared to single morphology [6, 7]. However, the limited application does not reflect the extensive usage, which emphasizes spouses' aspiration to enhance results and prevent miscarriage. Financially, PGT-A testing is a major hardship, with a typical extra bill of $5,000 to the already substantial additional market cost of IVF [8]. Patients lose time while waiting for findings, the embryology system increases, and there are ongoing concerns about the long-term implications of assisted hatching and trophectoderm sampling on the embryo. Utilization requires either an embryo transfer from a frozen embryo bank or from a fresh embryo bank that has not yet been tested due to the time required for PGT-A testing, which involves extra drugs, ultrasounds, and a financial burden for patients [9].

After embryo mosaicism has recently been affecting PGT-A data, it is being questioned, making it difficult for patients and doctors to store, handle, and use these embryos. PGT-A testing is not ideal when considering potential sequencing errors, inadequate sampling that may require re-biopsy, and mosaicism issues [10]. Techniques for non-invasive genetic testing, including Spent Culture Media (SCM), Blastocoel Fluid Sampling (BFS), and Artificial Intelligence (AI), are rapidly expanding in the field in response to these flawed invasive biopsy techniques [11]. These techniques can help overcome the issues in clinical maintenance. SCM test entails collecting the spent medium from prolonged embryo culture and determining the embryos' ploidy status utilizing cell-free DNA testing. Even though SCM is non-invasive and keeps embryos intact, standard trophectoderm biopsy always comes out on top in a head-to-head comparison. The only problem is that there isn't yet diagnostic consistency with SCM [12]. Contrast with trophectoderm biopsy or whole embryo sequencing yields results ranging from 30.4% to 90%. BFS uses blastocoel fluid aspiration with a needle to provide a different genetic material derived from non-cellular sources. Despite being lesser intrusive than trophectoderm biopsy, the method had worse predictive outcomes than SCM and presents several technical difficulties during sample collection and processing [13]. Technical issues related to poor DNA quality and quantity primarily restrict the accuracy of BFS and SCM testing, keeping these methods far from being deemed useful for commercial applications. When selecting embryos for transfer, vitrification, or disposal, these procedures are not a trustworthy way to test due to the wide range of accuracy in the findings [14].

AI, the application of ML to complex tasks previously requiring human intellect, has sparked rising interest in reproductive embryology owing to its potential to enhance clinical pregnancy outcomes, like implantation prediction and reduce subjectivity in embryo morphology grading [15-18]. When blastocyst images are analyzed with patient metadata like age and test findings, previous image-based AI algorithms have demonstrated encouraging results in euploidy prediction. From this perspective, Jiang et al. [19] investigated the AI model as a non-intrusive technique to categorize embryos as either euploid or aneuploid. To improve the accuracy of forecasting the ploidy status of embryos, scientists combined images of blastocysts with patient data and employed a voting ensemble consisting of CNNs, Support Vector Machines (SVMs), and Neural Networks (NNs) to make predictions. Similarly, Sun et al. [20] created the AI model by merging image-based CNN features and patient data to evaluate human IVF-derived embryos. They employed the UNet to segment embryo pictures, which were then categorized as euploid or aneuploid embryos using the ResNet50.

These models often rely on abundant labeled data or images, disregarding the potential benefits of a broader variety of clinical, demographic, and procedural aspects for embryo selection in IVF outcome predictions. The lack of sufficient embryo images can impact the model training and prediction performance. In recent years, GAN models have been developed to solve this issue, making it possible to create synthetic embryo pictures that closely mimic the distribution of actual data [21]. In human embryo image assessment, Dirvanauskas et al. [22] developed a Human Embryo Image Generator (HEMIGAN) using a GAN structure to produce photographs of human embryos at various developmental phases, and Cao et al. [23] configured StyleGAN to create high-fidelity blastocyst-stage embryo images. However, these models were restricted to creating images with limited resolution to lower the computational overhead and resource-intensive training nature of GAN, which resulted in poor image quality.

Hence, this manuscript develops a new AI framework called CSSGAN with MENB7 for embryo quality assessment. In this framework, the CSSGAN is intended to improve the GAN model's efficiency in generating human embryo pictures. This model uses pretrained weights and data augmentation to create many blastocyst-stage human embryo images. Besides, it adopts the new content-aware channel pruning and content-sensitive distillation approaches as a minimax optimization task to enrich the quality of the synthesized image. The channel-pruning reduces channels in the synthesis network while retraining the mapping network. The quantization procedure turns the model's floating-point values into integers, resulting in a much smaller model size and potentially faster computing. Distillation converts knowledge from a large, complicated model into a smaller, more efficient one. The pruning and distillation procedures are guided by a content-sensitive technique. With content awareness, it may efficiently prune channels that are unimportant to the contents of interest, such as non-embryo parts, resulting in dramatically improved embryo image quality. Once high-quality embryo pictures are obtained, they are fed into the Mask-RCNN for segmentation. The segmented pictures are then trained by EfficientNetB7 to capture the most significant features, which are then concatenated with patient information. These factors include the age of the mother, her AMH level, the quality of the father's sperm, and the total number of eggs that successfully fertilize. Moreover, the FC layer with softmax classifies the fused feature vector as euploid or aneuploid embryos. To summarize, this work primarily offers the following contributions:

- To design the CSSGAN technique for synthesizing high-quality and high-fidelity human embryo images with low computational complexity.
- To utilize the Mask-RCNN for segmenting the time-lapse embryo images for effective embryo morphology grading.
- To adopt the MENB7 model for concatenating the characteristics of embryo images and patient information efficiently during the prediction process, resulting in high accuracy.
- To assess the CSSGAN-MENB7 model's performance with the conventional AI models using distinct datasets in embryo ploidy status prediction.

The sections below are organized as follows: Section 2 studies earlier methods. Section 3 explains the CSSGAN-MENB7 model. Section 4 shows experimental outcomes. Section 5 summarizes the study and recommends further enhancements.

2. Literature Survey

Lee et al. [24] studied an end-to-end DL system for identifying ploidy status in raw time-lapse footage. First, raw videos and embryo information were obtained. The optical flows were then calculated by extracting frames at roughly 0.5 hours post-insemination (hpi) intervals. Data augmentation was used based on flipping, rotating, and contrast modification. Furthermore, a 2-stream Inflated 3D (I3D) ConvNet pretrained on ImageNet and Kinetics was fine-tuned and trained to forecast ploidy status into two groups: aneuploidy and euploidy. However, data provided from a single center lacks heterogeneity, which influences DL efficiency.

Thirumalaraju et al. [25] analyzed CNN models such as InceptionV3, ResNet50, Inception-ResNetV2, NASNetLarge, ResNeXt101, ResNeXt50, and Xception to categorize embryo pictures according to their morphological quality at 113 hours hpi. However, the accuracy

was low due to the insufficient data. To predict the ploidy status of embryos from time-lapse data, Huang et al. [26] utilized the 3D-ResNet50 with a multi-source data fusion network. In contrast, the accuracy was degraded due to model overfitting and inadequate data.
Diakiw et al. [27] evaluated a robust AI-based technique to forecast the probability of embryo euploidy using the blastocyst images from various imaging systems undergoing IVF. This technique was based on the ensemble of ResNet50, DenseNet161, and DenseNet121. Also, knowledge distillation was used for model training. However, overfitting can exist due to a small dataset, leading to poor generalizability. To forecast human embryo euploidy using time-lapse morphokinetic data, De Gheselle et al. [28] examined ML methods such as Random Forest (RF), scikit-learn gradient boosting classifier, SVM, multivariate logistic regression (LR), and naïve Bayes. However, the insufficient amount of data has an impact on these algorithms' generalizability.
Danardono et al. [29] reported an embryo ploidy status categorization using computer-assisted morphological evaluation and ML and DL algorithms. First, image augmentation was used to capture segmented embryos, and feature retrieval was done by a Histogram of Oriented Gradients (HOG), followed by Principal Component Analysis (PCA). In addition, SVM, RF, Decision Tree (DT), gradient boosting, and CNN were employed for prediction. However, the prediction performance was impacted by the limited quantity of data.
Barnes et al. [30] developed a non-invasive, automated embryo evaluation method to determine embryo ploidy status. First, time-lapse videos were retrieved, and each embryo was assigned a single static picture taken at 110 hours, along with clinical data. The dataset was then pre-processed by manually detecting underexposed photos, and missing morphokinetic parameters were imputed using median imputation. Lasso and LRs were used on clinical data to estimate feature significance. After establishing feature relevance, picture features were retrieved from ResNet18 and concatenated with clinical information before being sent to a final FC layer to predict the likelihood of aneuploidy and euploidy. On the contrary, unused embryos were included in the dataset and reported as negative outcomes, which has the potential to skew the dataset and worsen model performance.
Paya et al. [31] developed a spatiotemporal framework to forecast ploidy status. They utilized CNN to capture the important characteristics from time-lapse video frames. The Bidirectional Long Short-Term Memory (BiLSTM) layer then received this information and processed the temporal relationships to form a low-dimensional feature vector. Furthermore, a Multi-Layer Perceptron (MLP) separated them into two groups: euploid and non-euploid embryos. However, the data quantity was small. Using time-lapse photos, Kalyani and Deshpande [32] created a novel ResNet-Gated Recurrent Unit (GRU) model to forecast blastocyst development from cleavage-stage human embryos. However, the models' accuracy and generalizability were limited by the small dataset.
A DL-embryo scoring system for non-intrusive aneuploidy recognition was introduced by Ma et al. [33]. They trained a DL network using clinical data and an intelligent Data Analysis (iDA) score. However, accuracy relies on the NGS analysis. Rajendran et al. [34] designed a ploidy recognition technique called BELA, which utilizes multitask learning for predicting ploidy status. Initially, time-lapse image frames were pre-processed using the Hough image transform and augmented by random rotation and horizontal flipping. Then, features were extracted from the pre-processed time-lapse images with a pre-trained VGG16 model. These characteristics were input into a multipurpose BiLSTM model that has been trained to anticipate blastocyst score in addition to other morphological scores annotated by embryologists. To predict the ploidy of the blastocysts, an LR technique was used.

Table 1: Summary of Previous Studies for Embryo Status Prediction

Ref. No.	Image capture device	Category of input data	Prediction models	Endpoint with embryo status	Performance
[24]	Time-lapse incubator	Video image from days 1-5	2-stream I3D ConvNet	Aneuploidy or euploidy	AUC = 0.74
[25]	Embryoscope and inverted brightfield microscopes	Static images at 113 hpi	InceptionV3, ResNET50, Inception-ResNetV2, NASNetLarge, ResNeXt101, ResNeXt50, and Xception	Blastocyst and non-blastocysts	Accuracy = 90.97%; Recall = 93.69%; AUC = 0.89
[26]	Embryoscope+	Sequential images from time-lapse videos at 26-28 h, 40-45 h, 55-65 h, 85-95 h, 110-116 h, 132.5-136 h hpi, patient age, and kinetic parameters	3D-ResNet50	Euploid, aneuploid	AUC = 0.80; Accuracy = 78.5%
[27]	Microscope and embryoscope	Static 2D images of day 5 blastocysts	Ensemble ResNet50, DenseNet161, and DenseNet121	Euploid and aneuploid	Accuracy = 77.4%; Recall = 74.6%; AUC = 0.68
[28]	Embryoscope and Embryoscope+	Morphokinetic features, standard embryonic development features, demographic, and clinical data	RF classifier	Euploid and aneuploid	Accuracy = 72%; Precision = 66%; Recall = 88%; F1-score = 76%; AUC = 0.75
[29]	MIRI time-lapse incubator and inverted microscope	Time-lapse video, retrospective data, and static embryo images	Gradient boosting with HOG-PCA	Aneuploid or euploid	Accuracy = 0.74; Precision = 0.83; Recall = 0.84
[30]	Embryoscope+	Static images at 110 hours after hpi, patient age, morphological assessment, and morphokinetics	ResNet18	Probability of aneuploid and euploid	AUC = 0.761; Accuracy = 69.3%
[31]	Time-lapse incubator	Time-lapse videos from 10-115 hours after hpi	CNN-MLP	Euploid and non-euploid	Accuracy = 0.7308; Precision = 0.8205; Recall = 0.6957; F1-score = 0.7402
[32]	Time-lapse incubator	Time-lapse images from 0-72 h hpi	ResNet-GRU	Blastocyst and non-blastocyst	Accuracy = 93.05%; Recall = 0.97; AUC = 0.95
[33]	Embryoscope+	Time-lapse videos of blastocysts from days 5 to 7, clinical data, and embryonic features	iDA score-based DL network	Euploid, aneuploid, and mosaic	AUC = 0.688
[34]	Embryoscope	Time-lapse video sequences from 96-112 hours after hpi, patient age, and morphokinetics	VGG19-BiLSTM-LR	Aneuploid or euploid	AUC = 0.76
[35]	Time-lapse incubator	Sequential images from time-lapse videos (3-10 hours before biopsy)	U-Net, EfficientNetB6, ResNet50V2, and InceptionV3	Euploid and aneuploid	Accuracy = 0.6484 (for EfficientNetB6), 0.6562 (for ResNet50V2), and 0.6699 (for InceptionV3)

Handayani et al. [35] suggested an improved DL based U-Net blastocyst segmentation with CNN for predicting ploidy status. The first step was to collect blastocyst images from the time-lapse recordings in sequential order. Then, the U-Net was used for segmenting blastocyst images, which were further classified by the EfficientNetB6, ResNet50V2, and InceptionV3 into aneuploidy and euploidy. Table 1 provides a summary of these embryo status prediction models.

According to this literature, it is addressed that all the above-mentioned current models rely heavily on a small quantity of data or embryo pictures. This leads to overfitting and poor generalizability in predicting embryo ploidy status. Also, low-quality embryo pictures can have a considerable influence on prediction accuracy. Although GAN-based variants such as HEMIGAN [22] and StyleGAN [23] have demonstrated promising approaches to embryo image augmentation or synthesis, they are still affected by significant constraints. These constraints include poor-quality output, a high computational burden, and no specific optimization of tasks for embryo ploidy prediction. Specifically, StyleGAN can generate realistic imagery of blastocysts, but its results are currently limited in resolution and fidelity on large-scale embryo datasets. To overcome these gaps, this paper suggests the CSSGAN-MEBN7 to augment the image of human embryos and predict the ploidy status of embryos. The CSSGAN model provides content-sensitive distillation, content-aware channel pruning, and content-wise quantization, effectively reducing the computational complexity of acquiring high-resolution embryo images. Moreover, compared to current augmentation models, CSSGAN is hybridized with EfficientNetB7, where it considers the clinical features of the patient, forming an end-to-end model that helps enhance the performance of predicting ploidy status.

3. Proposed Methodology

This section describes the CSSGAN-MENB7 model briefly. A schematic representation of this study is demonstrated in Fig. 1, which involves different processes, including data acquisition, embryo image augmentation using CSSGAN, embryo image feature extraction using EfficientNetB7, concatenation of morphological characteristics with the clinical attributes, followed by the FC layer with a softmax function for embryo ploidy status prediction.

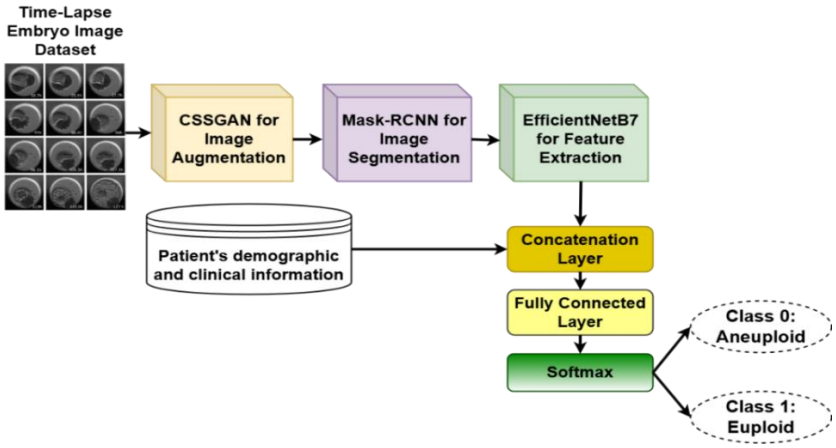

Fig. 1: Diagrammatic Representation of this Study

3.1 Dataset

In this study, time-lapse embryo images and clinical attributes (e.g., age, body mass index, tubal factor, pelvic factor, sperm count, etc.) contributed 85% and 15% of the model's predictive power. Therefore, the following datasets are considered for embryo ploidy status prediction:

1. **IVF/ICSI Dataset:** This dataset comprises 486 labeled records along with 29 attributes and an identifier for each patient that is either positive or negative. These data were gathered using a census approach from the fertility centers at Coimbatore, Tamil Nadu, between 2024 and 2025. Frozen embryo transfer cases were excluded; solely fresh embryo transfers were considered for data collection. There were 131 positive (euploid embryo) and 355 negative (aneuploid embryo) implantations. The attributes include the age of woman and man, body mass index, secondary fertility, tubal factor, pelvic factor, ovulatory factor, uterine factor, male factor, infertility duration, familiarity of IVF procedure, sperm count, sperm morphology, sperm motility, follicle stimulating hormone, anti-mullerian hormone, antral follicle counts, number of gonadotropin ampoules, total follicles in ultrasound, serum E2 level on the day of hCG administration, total retrieved oocytes, total oocytes of GV, MI, and MII qualities, type of treatment, embryo grade, total developed embryos, embryo transfer date, and number of transferred embryos.
2. **Time-lapse Embryo Dataset [36]:** This is a completely labeled dataset that includes 704 TLI videos of growing embryos with all seven focal planes accessible, totaling 2.4 million images. It includes high-resolution images, such as 500×500 time-lapse images capturing from fertilization (day 1) to blastocyst (day 5 or day 6) stages. Thus, this dataset covers 16 distinct developmental phases, including late cell divisions, periods following morulation, and very early phases. The community will be able to assess morphokinetic models for the first time with this publicly available dataset. This dataset is available at https://zenodo.org/records/6390798.

3.2 CSSGAN Model for Data Augmentation

The CSSGAN model is based on the StyleGAN structure and augments the number of time-lapse embryo images in training sets by synthesizing high-resolution embryo images. Its two main networks are Generator. G and Discriminator D, as shown in Fig. 2. Fig. 3 portrays the generator and discriminator network structures of the proposed CSSGAN model for high-fidelity embryo image generation.

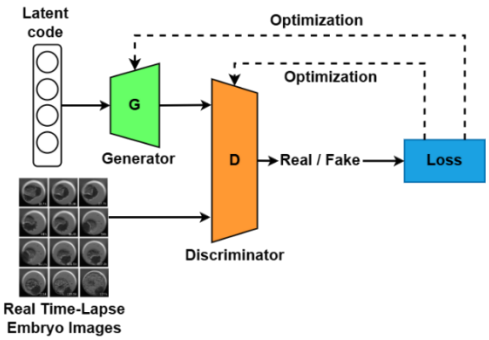

Fig. 2: StyleGAN-Based Embryo Image Augmentation

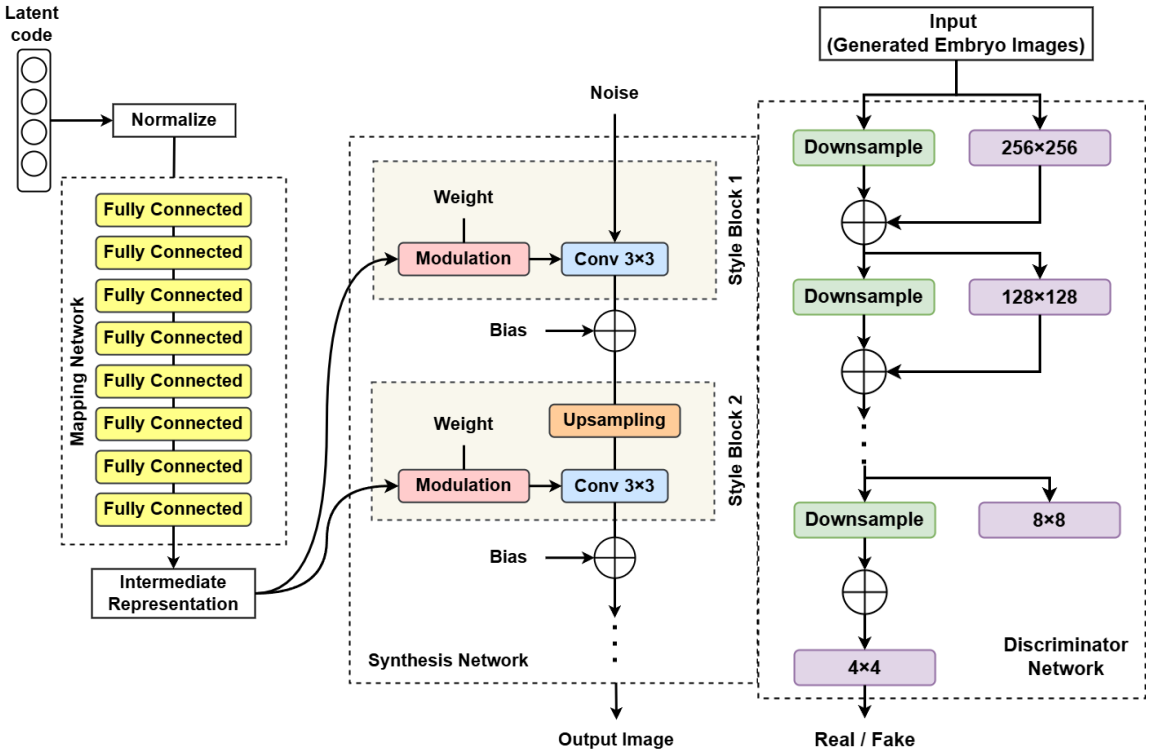

Fig. 3: (a) Structure of Generator and **Fig. 1:** (b) Discriminator Network in CSSGAN Model

While D seeks to distinguish between actual embryo images x and those generated by $(G(z))$, GThe objective is to generate synthetic embryo images that effectively trick D. Consider a solid full-precision generator. (G_0), that transforms the embryo images $\mathcal{X}$ to a latent space $\mathcal{Y}$ To create new, high-quality, high-fidelity embryo images, the objective is to discover a robust generator G from G_0, such that their produced embryo images $\{G_0(x), x \in \mathcal{X}\}$ and $\{G(x), x \in \mathcal{X}\}$ Have similar style transfer qualities (i.e., preserving morphological features). The goal of CSSGAN is formulated based on the standard minimax optimization dilemma in GAN as:

$$\min_G \max_D L_{GAN} = E_{y\in Y}\left[\log(D(y))\right] + E_{x\in X}\left[\log\left(1\text{-}D(G(x))\right)\right] \quad (1)$$

D Is the discriminator that was simultaneously trained by minimax optimization with a resilient generator G In Eq. (1), there is no need to compress. D because G Is the functional component that will be installed on computing devices, and D May be eliminated following training. The principle of content-sensitive distillation is used to induce the small generator. D to behave like the real big generator G_0 by adding a content-sensitive distillation loss term (L_{dist}), where $d(\cdot,\cdot)$ It is the Euclidean distance measure.

$$L_{dist} = E_{x\in X}\left[d(G(x), G_0(x))\right] \quad (2)$$

This study proposes to concurrently infer the G structure and the content-sensitive distillation process to accurately describe the architecture of G. Specifically, consider that. G can be reduced from G_0 By quantization and content-aware channel pruning. The trainable scale variables γ In the normalization layers, they are subjected to L_1-norm for content-aware channel pruning, which promotes channel sparsity: $L_{cp} = \|\gamma\|_1$. The content-aware channel pruning is applied using this sparsity restriction to the content-sensitive distillation loss in Eq. (2), where W stands for all other trainable weights in G.

$$L_{dist}(W,\gamma) + \rho L_{cp}(\gamma) = E_{x\in X}\left[d(G(x;W,\gamma), G_0(x))\right] + \rho\|\gamma\|_1 \quad (3)$$

In Eq. (3), ρ denotes the tradeoff variable, which handles the network sparsity leel. In addition, two quantiers, such $q_a(\cdot)$ and $q_w(\cdot)$, ere reused to quantize weights and activations, respectively, to combine quantization. Although adopting learnable quantization intervals is entirely possible, regular quantizrs with pre-etablished bitquantization $q_a(\cdot)$, $q_w(\cdot)$. Generators with activation quantiatio $q_a(\cdot)$ are

represented by G_q, whereas quantized weights are represened by $q_w(W)$. Accordingly, Eq. (4) represents the goal of combining content-sensitive distillation, content-aware channel pruning, and quantization:

$$L(W,\gamma,\theta)=L_{GAN}(W,\gamma,\theta)+\beta L_{dist}(W,\gamma)+\rho L_{cp}(\gamma)=E_{y\in Y}\left[\log\left(D(y;\theta)\right)\right]+E_{x\in X}\left[\log\left(1-D\left(G_q\left(x;q_w(W),\gamma\right);\theta\right)\right)\right]+E_{x\in X}\left[\beta d\left(G_q\left(x;q_w(W),\gamma\right),G_0(x)\right)\right]+\rho\|\gamma\|_1 \quad (4)$$

In Eq. (4), θ Are the variables in D. β,d are the content-sensitive distillation components, and $\rho\|\gamma\|_1$ is the content-aware channel pruning. In a minimax optimization framework, this CSSGAN target objective in Eq. (4) is resolved as follows:

$$\min_{W,\gamma}\max_{\theta} L(W,\gamma,\theta) \quad (5)$$

Three categories can be used to characterize the challenges of optimizing Eq. (5): (i) the problem with minimax optimization is already inherent; (ii) non-differentiable quantization procedures are involved in updating W; and (iii) another non-differentiable sparse loss term is involved in updating γ. These optimization procedures are explained in the sections below.

Updating $\boldsymbol{W}$: The further issues of revising W in Eq. (5) is defined by

$$\min_{W} L_W(W)=E_{x\in X}\left[\log\left(1-D\left(G_q\left(x;q_w(W),\gamma\right);\theta\right)\right)+\beta d\left(G_q\left(x;q_w(W),\gamma\right),G_0(x)\right)\right] \quad (6)$$

Determining $\nabla_W \mathcal{L}_W$ is crucial for solving Eq. (6) using gradient-based approaches, but it is challenging since $q_a(\cdot)$ and $q_w(\cdot)$ are non-differentiable. The definition of the concrete form of $q_a(\cdot)$ and $q_w(\cdot)$ shows how to backpropagate via them to find $\nabla_W L_W$. This research only examined how $q_a(\cdot)$ and $q_w(\cdot)$ operate on scalars because they are both elementwise operations. Here, a and w stand for a scalar portion in convolution and activation kernel tensors.

Activations are primarily clamped within the range [0,p] to constrain the values for quantizing them. The floating-point number is then converted to m-bit integers using $s_a={}^{p}/_{2^m}$, where m=8, as a scaling factor: $\text{round}\left({}^{\min(\max(0,a),p)}/_{s_a}\right)$. Consequently, the following is the activation quantization operator:

$$q_a(a)=\text{round}\left({}^{\min(\max(0,a),p)}/_{s_a}\right)\times s_a \quad (7)$$

Weights are quantized to n bits using balanced encoding for positive and negative intervals while maintaining the range of the first weights. In particular, the scale factor $s_w={}^{\|w\|_\infty}/_{2^{(n-1)}}$, which yields the weight quantization operator as:

$$q_w(w)=\text{round}\left({}^{w}/_{s_w}\right)\times s_w \quad (8)$$

During the reversal pass, a proxy called the straight-through estimator is employed as the pseudo gradient, as non-differentiability is shared by both quantization operators. To quantify activation, utilize

$$\frac{\partial q_a(a)}{\partial a}=\begin{cases}1, & \text{if } 0\le a\le p\\ 0, & \text{or else}\end{cases} \quad (9)$$

Likewise, the pseudo gradient for the weight quantization is allocated to

$$\frac{\partial q_w(w)}{\partial w}=1 \quad (10)$$

The derivatives of $q_a(\cdot)$ and $q_w(\cdot)$ are defined to determine $\nabla_W L_W$ by backpropagation, and W is updated with an Adam optimizer.

Updating γ: Revising γ Eq. (4) presents a non-conventional fidelity term, making it a sparse optimization challenge.:

$$\min_{\gamma} L_\gamma(\gamma)+\rho\|\gamma\|_1 \quad (11)$$

$$\text{Where } L_\gamma(\gamma)=E_{x\in X}\left[\log\left(1-D\left(G_q\left(x;q_w(W),\gamma\right);\theta\right)\right)+\beta d\left(G_q\left(x;q_w(W),\gamma\right),G_0(x)\right)\right] \quad (11a)$$

The proximal gradient is utilized to update γ as follows:

$$g_\gamma^{(t)}\leftarrow\nabla_\gamma L_\gamma(\gamma)|_{\gamma=\gamma^{(t)}} \quad (12)$$

$$\gamma^{(t+1)}\leftarrow\text{prox}_{\rho\eta^{(t)}}\left(\gamma^{(t)}-\eta^{(t)}g_\gamma^{(t)}\right) \quad (13)$$

In Eqns. (12)-(13), At step t, $\gamma^{(t)}$ represents the value of γ, while $\eta^{(t)}$ denotes the learning rate η. The proximal function $\text{prox}_\lambda(\cdot)$ associated with the l_1 A constraint is defined as the soft threshold function:

$$\text{prox}_\lambda(x)=\text{sgn}(x)\odot\max(|x|-\lambda 1,0) \quad (14)$$

In Eq. (14), ⊙ refers to the element-wise product, sgn(·) and max(·,·) refer to the element-wise sign and maximum functions.

Updating θ: The gradient ascent approach solves the linear maximization conundrum in Eq. (5), which is connected to updating θ:

$$\max_{\theta} L_{\theta}(\theta) = E_{y\in Y}\left[\log\left(D(y;\theta)\right)\right] + E_{x\in X}\left[\log\left(1-D\left(G_q(x);\theta\right)\right)\right] \quad (15)$$

The D (parameterized by θ) and G (parameterized by W and γ) are iteratively updated utilizing a history of generated embryo images.

3.2.1 Implementation of CSSGAN Model

Given the gradient computation, the final remaining component in addressing issue Eq. (4) is to pick d. Content-sensitive distillation aims to reduce the difference between two sets of produced embryo pictures for StyleGAN compression. Additionally, the perceptual loss is chosen for d. It has been widely used to regularize CSSGAN-based embryo picture creation and has demonstrated efficacy in measuring both low-level visual cues and high-level semantic discrepancies across embryo images. The pseudocode for CSSGAN with end-to-end optimization is summarized in Algorithm 1. In the time-lapse embryo dataset, for each video, approximately 3415 high-fidelity and high-quality time-lapse embryo images are generated using the CSSGAN, of which 2732 images per video were used for training and 683 for testing.

Algorithm 1: CSSGAN Model Training

Input: $X,Y,\beta,p,T,\{\alpha^{(t)}\}_{t=1}^{T},\{\eta^{(t)}\}_{t=1}^{T}$

Output: W,γ

1. Begin
2. Randomly initialize $W^{(1)},\gamma^{(1)},\theta^{(1)}$;
3. for(t←1:T)
4. Obtain a batch of embryo image data from X and Y;
5. $W^{(t+1)}\leftarrow W^{(t)}-\alpha^{(t)}\nabla_W L_W$;
6. $\gamma^{(t+1)}\leftarrow \mathrm{prox}_{\rho\eta^{(t)}}\left(\gamma^{(t)}-\eta^{(t)}\nabla_\gamma L_\gamma(\gamma)\right)$;
7. $\theta^{(t+1)}\leftarrow \theta^{(t)}+\alpha^{(t)}\nabla_\theta L_\theta$;
8. $end\ for$
9. $W\leftarrow q_w\left(W^{T+1}\right)$;
10. $\gamma\leftarrow\gamma^{T+1}$;
11. End

3.3 Mask-RCNN

The generated embryo images are segmented by the Mask-RCNN, which incorporates the Feature Pyramid Network (FPN) and Region of Interest Alignment (ROIAlign). The basic architecture of Mask-RCNN is shown in Fig. 4, which comprises the backbone network, FPN, Regional Proposal Network (RPN), ROIAlign, bounding box, and mask branch. The image segmentation begins by inputting the picture to be processed as the pre-trained ResNet50 + FPN, which extracts features and generates feature maps. Through RPN, a significant number of candidate frames (ROI) are obtained for the feature map. The softmax classifier is then used for binary classification of the background and foreground. Frame regression yields more precise position details for the candidate's frame. Furthermore, non-maximum suppression filters out a portion of the ROI. Each ROI can then create a fixed-size feature map once the feature map and the final ROI are submitted in the RoIAlign layer. The feature map is finally delivered to the Fully Convolutional Network (FCN) to create binary mask predictions for every embryo picture and FC layer to obtain the boundary box along with the class label.

Classification loss (L_{cls}), regression loss (L_{box}), and segmentation loss (L_{mask}) are the three parameters that establish the loss function of Mask-RCNN as follows:

$$L_{Mask\text{-}RCNN}=L_{cls}+L_{box}+L_{mask} \quad (16)$$

The total loss function is computed as:

$$L_{total}=L_{RPN}+L_{Mask\text{-}RCNN} \quad (17)$$

In Eq. (17), $\mathcal{L}_{RPN}$ is the RPN loss value.

3.4 EfficientNetB7

The pre-trained EfficientNetB7 is then used to extract morphological characteristics from the segmented embryo pictures. To lower the computing cost by a factor of f^2, where f is the filter size, the EfficientNetB7 was constructed using Mobile-inverted Bottleneck Convolution (MBConv) units, which utilize kernel scales of 3×3 and 5×5. This compound scaling technique consistently adjusts the network's breadth, depth, and resolution. Using the transfer learning methodology, this network can extract the salient characteristics. As depicted in Fig. 5, this network consists of the following layers:

- First, the input layer receives embryo picture segments with the dimension 600×600, and the convolution (conv) layer processes those pictures.
- Then, EfficientNet blocks use depthwise convolution to convolve each input channel individually with 3×3 and 5×5 learnable filters.

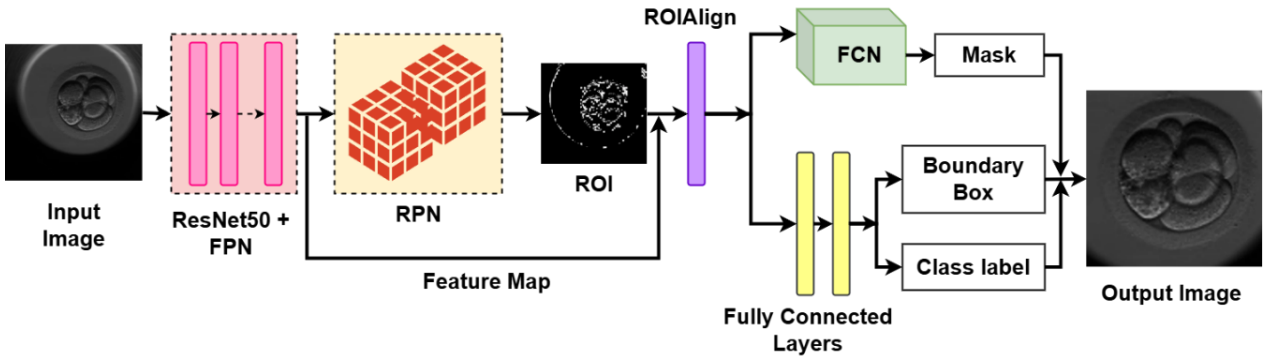

Fig. 4: Structure of Mask-RCNN for Embryo Image Segmentation

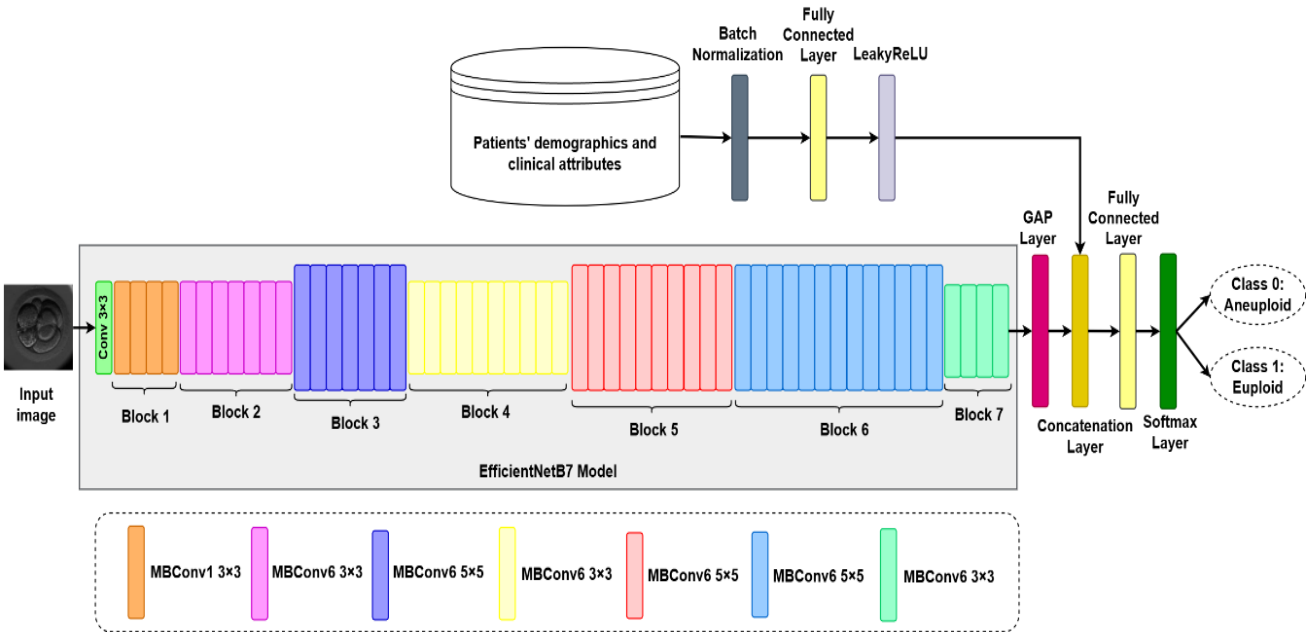

Fig. 5: Structure of EfficientNetB7 for Embryo Ploidy Prediction

- The Global Average Pooling (GAP) layer reduces feature map spatial dimensionality to 1×1, decreasing overfitting and enhancing generalization.
- To obtain a high-level feature representation, the patient's demographics and clinical attributes are also supplied to the batch normalization, FC layer (where the number of neurons corresponds to the input information), and Leaky Rectified Linear Unit (LeakyReLU) activation layer.
- Moreover, the concatenation layer combines the extracted morphological features and high-level representation of patient data to create a unified feature vector.
- A FC layer with neurons equal to the total classes is concatenated, followed by a softmax function to estimate probabilities for each class (euploid and aneuploid embryos).

The pseudocode for the entire CSSGAN-MENB7 model for predicting embryo ploidy status is summarized in Algorithm 2.
Algorithm 2: Proposed CSSGAN-MENB7 Model for Embryo Ploidy Status Prediction
Input: Time-lapse embryo image dataset and IVF/ICSI dataset
Output: Classified embryos as euploid or aneuploid
1. Begin
2. Split the datasets into training and test with a ratio of 8:2;
3. for(clinical attributes in training IVF/ICSI dataset)
4. Provide them to the batch normalization, FC, and LeakyReLU;
5. Obtain the high-level feature representations;
6. end for
7. for(embryo images in the training dataset)
8. Train the CSSGAN as Algorithm 1;
9. Generate high-quality, high-fidelity embryo images;
10. Train the Mask-RCNN model using the generated images;
11. Obtain the segmented ROI for each embryo image;
12. Feed the embryo ROI images into the EfficientNetB7 model;
13. Process the conv, MBConv, and GAP layers to capture the morphological features;
14. end for
15. Concatenate the high-level feature representations of clinical data and morphological features to get a unified feature vector;
16. Train the FC layer with a softmax function for classification;
17. Use the trained model to predict ploidy status as euploid or aneuploid embryos from the test data;

18. Evaluate the model performance.
19. End

4. Experimental Results

This section evaluates the CSSGAN-MENB7 model's performance compared to the previous models, such as Voting Ensemble [19], ResNet18 [30], CNN-MLP [31], ResNet-GRU [32], and EfficientNetB6 [35], using the datasets described in Section 3.1. The experiments were executed on a laptop with an Intel i7 processor, 8GB RAM, 1TB HDD, and Windows 10 64-bit OS. The proposed CSSGAN-MENB7 and existing models were implemented using Python 3.12.4. The hyperparameters were initialized randomly and optimized by the Adam optimizer, with the initialization of hyperparameters listed in Table 2.

Table 2: Hyperparameter Settings

Parameters	Values
Voting Ensemble [19], ResNet18 [29], CNN-MLP [30], ResNet-GRU [31], and EfficientNetB6 [34], and Proposed CSSGAN-MENB7	
β_1, β_2 in Adam optimizer	0.9, 0.5
Batch size	64
Dropout rate	0.5
Epochs	100
Learning rate	0.001
Loss function	Cross-entropy loss
Momentum	0.9
Optimizer	Adam
CNN-MLP [30]	
Activation function	Sigmoid
No. of hidden layers	2
Number of neurons in each hidden layer	128
Proposed CSSGAN-MENB7	
Activation clamping threshold p	4
No. of iterations	5000
Latent vector dimension	512

4.1 Performance Metrics

Accuracy: It defines the fraction of occurrences that are exactly categorized. It is determined by

$$Accuracy = \frac{True\ Positive\ (TP) + True\ Negative\ (TN)}{TP + TN + False\ Positive\ (FP) + False\ Negative\ (FN)} \tag{18}$$

In Eq. (28), TP represents the number of euploid embryos exactly categorized as euploid (i.e., positive); TN is the number of aneuploid embryos exactly categorized as aneuploid (i.e., negative); FP represents the number of aneuploid embryos inexactly categorized as euploid, and FN is the number of euploid embryos inexactly categorized as aneuploid.

Recall: It is the proportion of exactly categorized data in the total positive class, as:

$$Recall = \frac{TP}{TP + FN} \tag{19}$$

Precision: It is also called Positive Predictive Value (PPV), which measures the fraction of positive data that are euploid, as:

$$Precision = \frac{TP}{TP + FP} \tag{20}$$

F1-score: It is the weighted average of precision and recall, as:

$$F1 - \text{score} = \frac{2 \times Precision \times Recall}{Precision + Recall} \tag{21}$$

Receiver Operating Characteristic – Area Under the Curve (ROC-AUC): It plots the TPR against the FP Rate (FPR) at various threshold settings. It determines the capability of the method to differentiate between positive and negative classes. The FPR is determined as:

$$FPR = \frac{FP}{FP + TN} \tag{22}$$

Area Under the Precision-Recall Curve (AUPRC): It determines the relationship between Precision and Recall (PR) and provides it in a unified value.

The proposed CSSGAN-MENB7 model predicts euploid and aneuploid status using both IVF/ICSI clinical attributes and time-lapse embryo images of 486 patients. For this purpose, attributes from the IVF/ICSI dataset and time-lapse video frames were split into an 80:20 ratio for training and testing. Therefore, 105 positive and 284 negative patient cases were used for training, while 26 positive and 71 negative patient cases were used for testing. Fig. 6 presents the confusion matrix of the CSSGAN-MENB7 model on the test dataset for embryo ploidy status prediction. It demonstrates that the CSSGAN-MENB7 model performs well in predicting euploid and aneuploid embryos using both IVF attributes and time-lapse embryo images.

4.2 Performance Analysis of CSSGAN with Other GAN Models for Image Augmentation

This section evaluates the efficiency of CSSGAN with standard GAN models, including GAN-(feature mapping), HEMIGAN [22], and StyleGAN [23], using Frechet Inception Distance (FID) and Kernel Inception Distance (KID). FID scores assess the variance between produced and actual embryo pictures, with lower scores suggesting greater alignment. KID scores are compensation measures for FID that quantify the similarity between real and produced pictures. Lower KID scores signify a greater similarity. Fig. 7 exhibits some samples of time-lapse embryo images produced by the CSSGAN model.

Fig. 8 shows the FID scores for several GAN models across 5000 iterations. All models' FID curves showed similar tendencies, with FID values gradually declining over subsequent training rounds. As training continues, the FID value constantly decreases, indicating a continuing improvement in image quality. The GAN, HEMIGAN, and StyleGAN began with significantly high FID scores of 200.0, 170.0, and 130.0, respectively, showing considerable differences between their initial and actual embryo pictures.

Testing Set			
Actual / Predicted	Euploid	Aneuploid	SUM
Euploid	24 24.74%	2 2.06%	26 92.31% 7.69%
Aneuploid	2 2.06%	69 71.13%	71 97.18% 2.82%
SUM	26 92.31% 7.69%	71 97.18% 2.82%	93 / 97 95.88% 4.12%

Fig. 6: Confusion Matrix of CSSGAN-MENB7 Model for Embryo Ploidy Status Prediction

Fig. 7: Samples of Time-Lapse Embryo Images Generated by CSSGAN

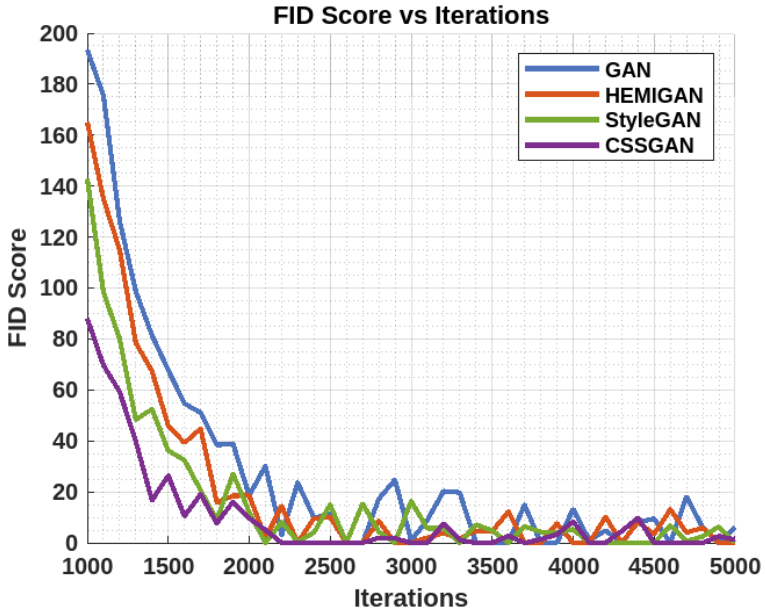

Fig. 8: FID Score vs. Iterations for CSSGAN and Other GAN Models

However, as training advances, the FID value constantly decreases, demonstrating that pre-trained weights make a significant contribution to producing high-quality pictures that resemble actual ones. During training, these models had a quick FID drop followed by stability. These models' respective FID scores after 5000 iterations were 3.66, 2.43, and 1.29. In contrast to the other models, the suggested CSSGAN started with a noticeably lower FID value of 90.0. This implies that embryo pictures that closely resemble the distribution of real images may be produced using CSSGAN, starting with pre-trained weights. Pretrained weights significantly contributed to producing high-quality

photographs that resembled actual ones, as seen by the FID value's continuous decline during training. After 5000 training rounds, the CSSGAN model's FID was 0.59. Thus, the CSSGAN can produce high-quality, high-fidelity embryo images compared to the other models effectively.

The KID scores for several GAN models over 5000 iterations are displayed in Fig. 9. Consistent patterns in the KID curves of each model showed a progressive decline in KID values with increasing training. The KID values steadily decreased in GAN, HEMIGAN, and StyleGAN, suggesting that the model is now better able to produce embryo samples that closely resemble actual ones. These models had KID scores of 0.00010, 0.000038, and 0.000008 after 5000 iterations, respectively. The CSSGAN model demonstrated a sharp decline in KID values as training went on, indicating significant improvement in producing more lifelike embryo pictures. The KID of this model was 0.0000016 following 5000 iterations.

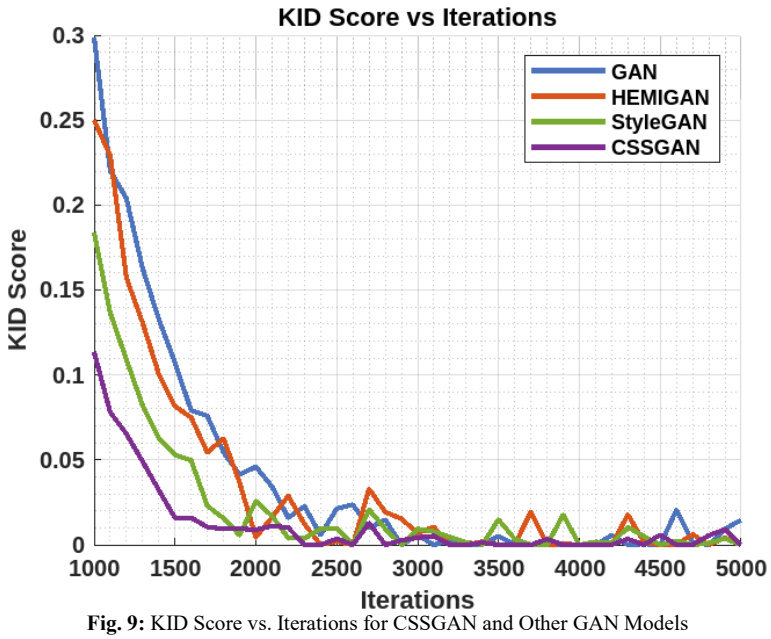

Fig. 9: KID Score vs. Iterations for CSSGAN and Other GAN Models

4.3 Performance Assessment of Suggested CSSGAN-MENB7 with Conventional Approaches

The performance outcomes of suggested and conventional methods in terms of different metrics are provided in Table 3.

Fig. 10 shows the accuracy of the CSSGAN-MENB7 model against current models for predicting embryo ploidy status. It is observed that the CSSGAN-MENB7 increases the accuracy by 13.15%, 9.49%, 6.39%, 2.04%, and 1.32% compared to the Voting Ensemble, ResNet18, CNN-MLP, ResNet-GRU, and EfficientNetB6, respectively. In Fig. 11, a performance analysis is shown in terms of precision. It indicates that the precision of the CSSGAN-MENB7 model is 12.72%, 9.1%, 6.7%, 2.83%, and 1.47% higher than the same current models.

Fig. 12 displays the recall results for proposed and existing models for embryo ploidy status prediction. It is addressed that the CSSGAN-MENB7 model increases the recall by 13%, 9.42%, 6.38%, 2.01%, and 1.31% compared to the same models. Similarly, F1-score comparison for proposed and existing models is demonstrated in Fig. 13. It observes that the CSSGAN-MENB7 improves the F1-score by 12.84%, 9.21%, 6.5%, 2.39%, and 1.36% compared to the current models.

Table 3: Performance Outcomes of Suggested and Conventional Approaches

Models	Accuracy	Precision	Recall	F1-score
Voting Ensemble	84.73	84.58	84.82	84.68
ResNet18	87.56	87.39	87.60	87.49
CNN-MLP	90.11	89.35	90.10	89.72
ResNet-GRU	93.95	92.72	93.96	93.32
EfficientNetB6	94.62	93.96	94.61	94.27
Proposed CSSGAN-MENB7	**95.88**	**95.34**	**95.85**	**95.55**

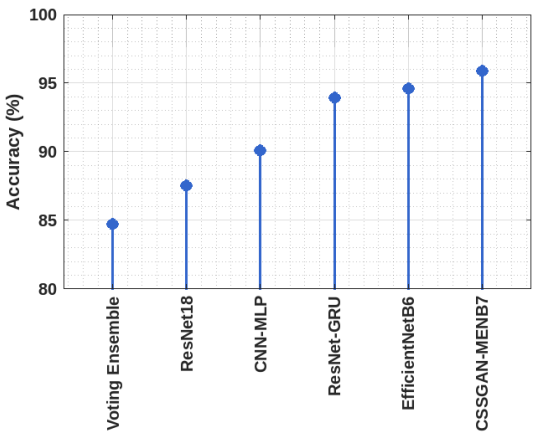

Fig. 10: Comparison of Accuracy

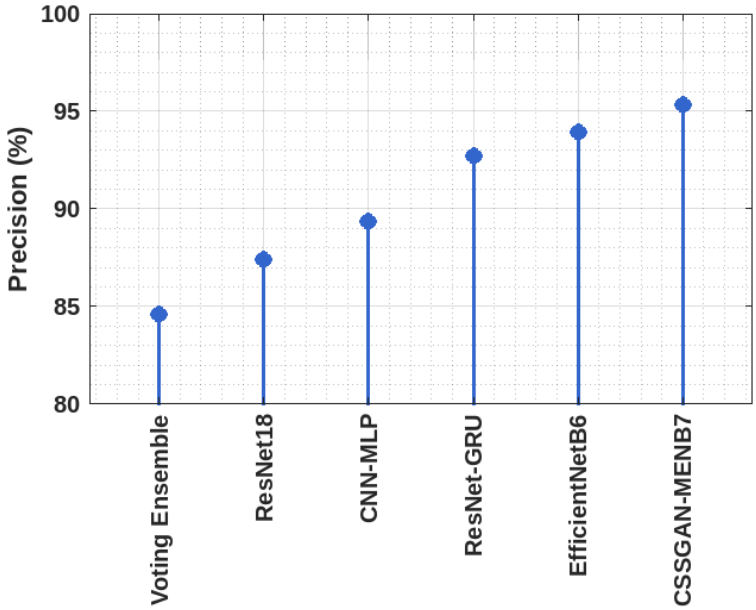

Fig. 11: Comparison of Precision

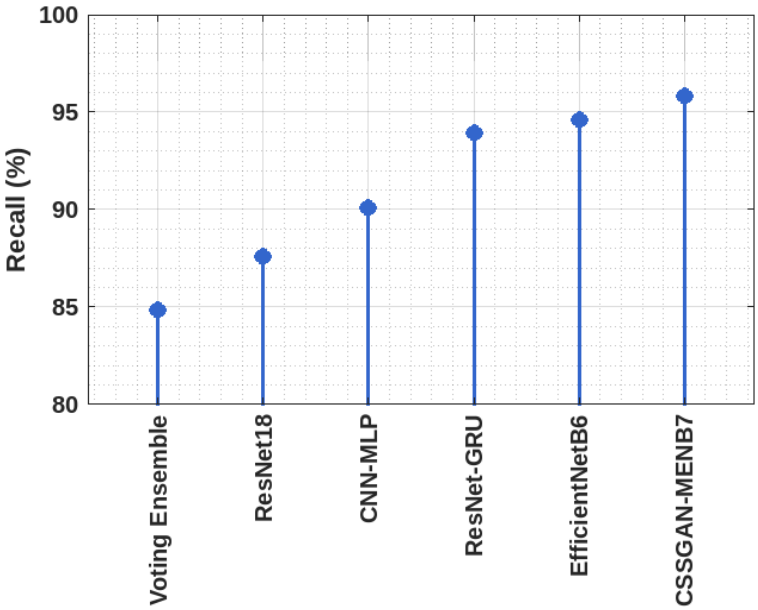

Fig. 12: Comparison of Recall

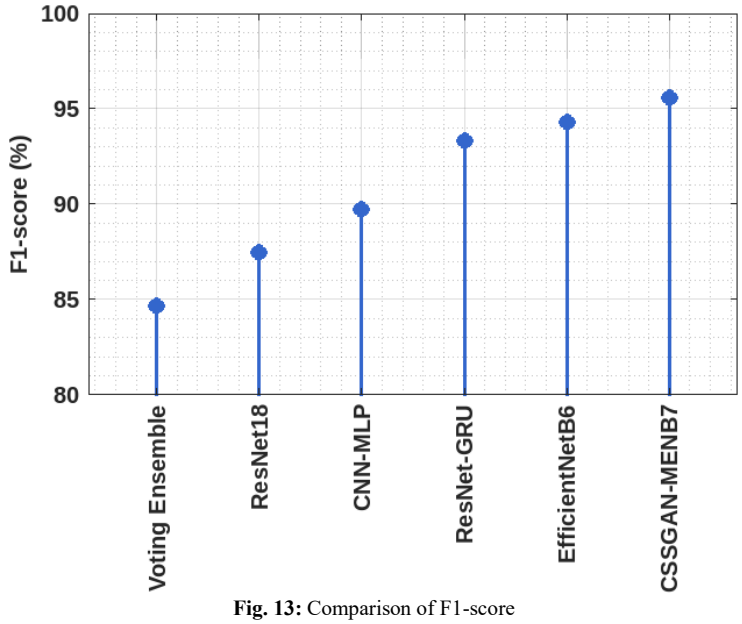

Fig. 13: Comparison of F1-score

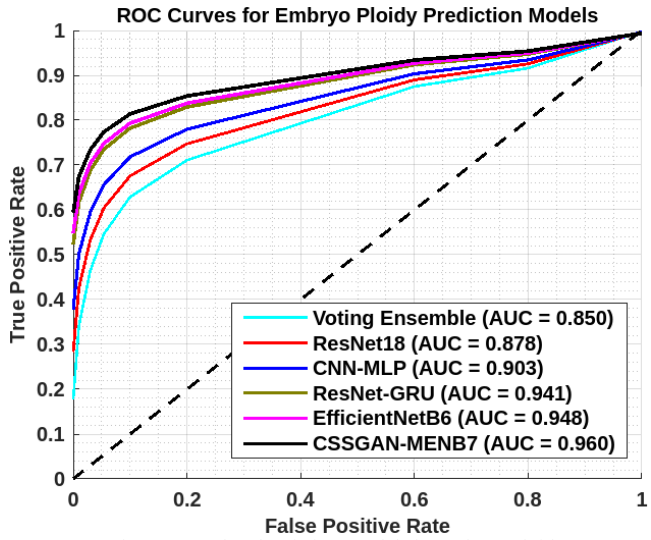

Fig. 14: ROC-AUC for Proposed and Existing Models in Embryo Ploidy Status Prediction

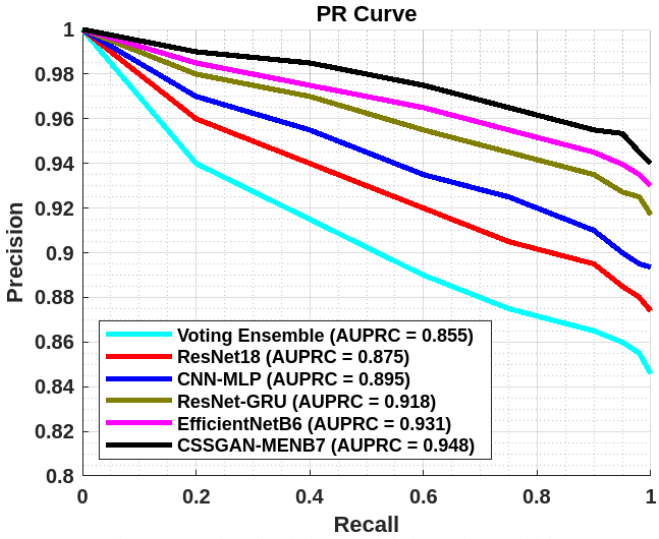

Fig. 15: PR Curve for Proposed and Existing Models in Embryo Ploidy Status Prediction

Fig. 14 shows the ROC curves for the CSSGAN-MENB7 and current models for embryo ploidy status prediction by combining time-lapse embryo images and clinical characteristics. Compared to the existing models, the CSSGAN-MENB7 model outperforms them all in terms of accuracy, precision, recall, F1-score, and AUC, all of which are at 0.96.

Fig. 15 depicts the PR curves for the suggested and conventional methods. The AUPRC curve is critical in understanding the efficacy of DL models in predicting embryo ploidy status, such as euploid and aneuploid, for successful IVF outcomes. It can demonstrate the suggested model's correct outcomes compared to earlier models. This is achieved by generating high-fidelity embryo images by the CSSGAN. These images are partitioned and learned to capture morphological features, which are then combined with the clinical attributes to predict embryo ploidy status. Moreover, the channel pruning and quantization approaches in CSSGAN reduce the computational complexity, resulting in the CSSGAN-MEBN7 model requiring approximately 3.2 hours for training on a 32GB GPU and less than 0.3 seconds per image for inference. This suggests the potential for optimization for deployment in resource-constrained IVF clinics.

5. Conclusion

The CSSGAN-MENB7 model is developed in this paper to recognize the embryo ploidy status to achieve successful IVF results. Initially, the CSSGAN used content-sensitive distillation and content-aware channel pruning as minimax optimization tasks to produce many high-quality, high-fidelity images of human embryos at the blastocyst stage. For segmentation, the produced pictures were sent into the Mask-RCNN. EfficientNetB7 then extracted the pertinent features from the segmented images and combined them with the clinical and demographic information of the patient to produce a single feature vector. Additionally, the ultimate prediction of euploid and aneuploid embryos was made using the FC layer with a softmax function. Lastly, the findings demonstrated that, in comparison to the traditional DL models, the CSSGAN-MEBN7 obtained 95.88% accuracy in predicting embryo ploidy status. Future work could focus on integrating the Internet of Things (IoT) with the CSSGAN-MENB7 model for real-time embryo ploidy status prediction, thus improving feasibility for IVF clinics.

References

[1] D.K. Gardner, D. Sakkas, Making and selecting the best embryo in the laboratory, Fertility and Sterility, 120(3) (2023) 457-466, available online: https://doi.org/10.1016/j.fertnstert.2022.11.007

[2] V. Lacconi, M. Massimiani, I. Carriero, et al., When the embryo meets the endometrium: identifying the features required for successful embryo implantation, International Journal of Molecular Sciences, 25(5) (2024) 2834, available online: https://doi.org/10.3390/ijms25052834

[3] A. Yazdani, I. Halvaei, C. Boniface, N. Esfandiari, Effect of cytoplasmic fragmentation on embryo development, quality, and pregnancy outcome: a systematic review of the literature, Reproductive Biology and Endocrinology, 22(1) (2024) 55, available online: https://doi.org/10.1186/s12958-024-01217-7

[4] J. Wang, Y. Guo, N. Zhang, T. Li, Research progress of time-lapse imaging technology and embryonic development potential: a review, Medicine, 102(38) (2023) e35203, available online: https://doi.org/10.1097/MD.0000000000035203

[5] K. Tvrdonova, S. Belaskova, T. Rumpikova, et al., Differences in morphokinetic parameters and incidence of multinucleations in human embryos of genetically normal, abnormal and euploid embryos leading to clinical pregnancy, Journal of Clinical Medicine, 10(21) (2021) 5173, available online: https://doi.org/10.3390/jcm10215173

[6] C. Morales, Current applications and controversies in preimplantation genetic testing for aneuploidies (PGT-A) in in vitro fertilization, Reproductive Sciences, 31(1) (2024) 66-80, available online: https://doi.org/10.1007/s43032-023-01301-0

[7] O.S. Davis, L.A. Favetta, S. Deniz, et al., Potential costs and benefits of incorporating PGT-A across age groups: a Canadian clinic perspective, Journal of Obstetrics and Gynaecology Canada, 46(5) (2024) 102361, available online: https://doi.org/10.1016/j.jogc.2024.102361

[8] A. Von Schondorf-Gleicher, L. Mochizuki, R. Orvieto, P. Patrizio, A.S. Caplan, N. Gleicher, Revisiting selected ethical aspects of current clinical in vitro fertilization (IVF) practice, Journal of Assisted Reproduction and Genetics, 39(3) (2022) 591-604, available online: https://doi.org/10.1007/s10815-022-02439-7

[9] Z.J. Pavlovic, G.E. Smotrich, E.P. New, et al., Fresh vs. frozen: pregnancy outcomes and treatment efficacy between fresh embryo transfer vs. untested freeze-all cycles, F&S Reports, 5(4) (2024) 369-377, available online: https://doi.org/10.1016/j.xfre.2024.09.003

[10] E. Moustakli, A. Zikopoulos, C. Skentou, I. Bouba, K. Dafopoulos, I. Georgiou, Evolution of minimally invasive and non-invasive preimplantation genetic testing: an overview, Journal of Clinical Medicine, 13(8) (2024) 2160, available online:

[11] A. del Arco de la Paz, C. Giménez-Rodríguez, A. Selntigia, M. Meseguer, D. Galliano, Advancements and challenges in preimplantation genetic testing for aneuploidies: in the pathway to non-invasive techniques, Genes, 15(12) (2024) 1613, available online: https://doi.org/10.3390/jcm13082160

[12] A. De Vos, N. De Munck, Trophectoderm biopsy: present state of the art, Genes, 16(2) (2025) 134, available online: https://doi.org/10.3390/genes16020134

[13] A. Sethi, N. Singh, R. Gupta, et al., P-725 role of non-invasive preimplantation genetic testing-aneuploidy (NIPGT-A) using spent culture media (SCM) and its concordance with Trophoectoderm (TE) biopsy: a prospective cohort study, Human Reproduction, 38(Supplement_1) (2023) dead093-1045, available online: https://doi.org/10.1093/humrep/dead093.1045

[14] R. Nuñez-Calonge, N. Santamaria, T. Rubio, J.M. Moreno, Making and selecting the best embryo in in vitro fertilization, Archives of Medical Research, 55(8) (2024) 103068, available online: https://doi.org/10.1016/j.arcmed.2024.103068

[15] M. Salih, C. Austin, R.R. Warty, et al., Embryo selection through artificial intelligence versus embryologists: a systematic review, Human Reproduction Open, 2023(3) (2023) hoad031, available online: https://doi.org/10.1093/hropen/hoad031

[16] Â. Ribeiro, A. Gomes, R. Magalhães, J. Amaral, J.S. Carvalho, Implementing artificial intelligence in the embryology laboratory: a methodological approach, Reproductive BioMedicine Online, 48 (2024) 104036, available online: https://doi.org/10.1016/j.rbmo.2024.104036

[17] K. Si, B. Huang, L. Jin, Application of artificial intelligence in gametes and embryos selection, Human Fertility, 26(4) (2023) 757-777, available online: https://doi.org/10.1080/14647273.2023.2256980

[18] V.S. Jiang, C.L. Bormann, Artificial intelligence in the in vitro fertilization laboratory: a review of advancements over the last decade, Fertility and Sterility, 120(1) (2023) 17-23, available online: https://doi.org/10.1016/j.fertnstert.2023.05.149

[19] V.S. Jiang, H. Kandula, P. Thirumalaraju, et al., The use of voting ensembles to improve the accuracy of deep neural networks as a non-invasive method to predict embryo ploidy status, Journal of Assisted Reproduction and Genetics, 40(2) (2023) 301-308, available online: https://doi.org/10.1007/s10815-022-02707-6

[20] L. Sun, J. Li, S. Zeng, et al., Artificial intelligence system for outcome evaluations of human in vitro fertilization-derived embryos, Chinese Medical Journal, 137(16) (2024) 1939-1949, available online: https://doi.org/10.1097/CM9.0000000000003162

[21] R. He, V. Sarwal, X. Qiu, et al., Generative AI models in time-varying biomedical data: scoping review, Journal of Medical Internet Research, 27 (2025) e59792, available online: https://doi.org/10.2196/59792

[22] D. Dirvanauskas, R. Maskeliūnas, V. Raudonis, R. Damaševičius, R. Scherer, Hemigen: human embryo image generator based on generative adversarial networks, Sensors, 19(16) (2019) 3578, available online: https://doi.org/10.3390/s19163578

[23] P. Cao, J. Derhaag, E. Coonen, et al., Generative artificial intelligence to produce high-fidelity blastocyst-stage embryo images, Human Reproduction, 39(6) (2024) 1197-1207, available online: https://doi.org/10.1093/humrep/deae064

[24] C.I. Lee, Y.R. Su, C.H. Chen, et al., End-to-end deep learning for recognition of ploidy status using time-lapse videos, Journal of Assisted Reproduction and Genetics, 38(7) (2021) 1655-1663, available online: https://doi.org/10.1007/s10815-021-02228-8

[25] P. Thirumalaraju, M.K. Kanakasabapathy, C.L. Bormann, et al., Evaluation of deep convolutional neural networks in classifying human embryo images based on their morphological quality, Heliyon, 7(2) (2021) e06298, available online: https://doi.org/10.1016/j.heliyon.2021.e06298

[26] B. Huang, W. Tan, Z. Li, L. Jin, An artificial intelligence model (euploid prediction algorithm) can predict embryo ploidy status based on time-lapse data, Reproductive Biology and Endocrinology, 19 (2021) 1-10, available online: https://doi.org/10.1186/s12958-021-00864-4

[27] S.M. Diakiw, J.M.M. Hall, M.D. VerMilyea, et al., Development of an artificial intelligence model for predicting the likelihood of human embryo euploidy based on blastocyst images from multiple imaging systems during IVF, Human Reproduction, 37(8) (2022) 1746-1759, available online: https://doi.org/10.1093/humrep/deac131

[28] S. De Gheselle, C. Jacques, J. Chambost, et al., Machine learning for prediction of euploidy in human embryos: in search of the best-performing model and predictive features, Fertility and Sterility, 117(4) (2022) 738-746, available online: https://doi.org/10.1016/j.fertnstert.2021.11.029

[29] G.B. Danardono, N. Handayani, C.M. Louis, et al., Embryo ploidy status classification through computer-assisted morphology assessment, AJOG Global Reports, 3(3) (2023) 100209, available online: https://doi.org/10.1016/j.xagr.2023.100209

[30] J. Barnes, M. Brendel, V.R. Gao, et al., A non-invasive artificial intelligence approach for the prediction of human blastocyst ploidy: a retrospective model development and validation study, The Lancet Digital Health, 5(1) (2023) e28-e40, available online: https://doi.org/10.1016/S2589-7500(22)00213-8

[31] E. Paya, C. Pulgarín, L. Bori, A. Colomer, V. Naranjo, M. Meseguer, Deep learning system for classification of ploidy status using time-lapse videos, F&S Science, 4(3) (2023) 211-218, available online: https://doi.org/10.1016/j.xfss.2023.06.002

[32] K. Kalyani, P.S. Deshpande, A deep learning model for predicting blastocyst formation from cleavage-stage human embryos using time-lapse images, Scientific Reports, 14(1) (2024) 28019, available online: https://doi.org/10.1038/s41598-024-79175-8

[33] B.X. Ma, G.N. Zhao, Z.F. Yi, Y.L. Yang, L. Jin, B. Huang, Enhancing clinical utility: deep learning-based embryo scoring model for non-invasive aneuploidy prediction, Reproductive Biology and Endocrinology, 22(1) (2024) 58, available online: https://doi.org/10.1186/s12958-024-01230-w

[34] S. Rajendran, M. Brendel, J. Barnes, et al., Automatic ploidy prediction and quality assessment of human blastocysts using time-lapse imaging, Nature Communications, 15(1) (2024) 7756, available online: https://doi.org/10.1038/s41467-024-51823-7

[35] N. Handayani, G.B. Danardono, A. Boediono, et al., Improving deep learning-based algorithm for ploidy status prediction through combined U-NET blastocyst segmentation and sequential time-lapse blastocysts images, Journal of Reproduction & Infertility, 25(2) (2024) 110, available online: https://doi.org/10.18502/jri.v25i2.16006

[36] T. Gomez, M. Feyeux, J. Boulant, et al., A time-lapse embryo dataset for morphokinetic parameter prediction, Data in Brief, 42 (2022) 108258, available online: https://doi.org/10.1016/j.dib.2022.108258.